SUBTASK 6.5 – SiAlON COATINGS OF SILICON NITRIDE AND SILICON CARBIDE

Final Topical Report

Prepared for:

AAD Document Control
U.S. Department of Energy
National Energy Technology Laboratory
PO Box 10940, MS 921-143
Pittsburgh, PA 15236-0940

Cooperative Agreement No. DE-FC26-98FT40320--17; UND Fund 4259
Performance Monitor: Udaya S. Rao

Prepared by:

Jan W. Nowok
John P. Hurley
John P. Kay

Energy & Environmental Research Center
University of North Dakota
PO Box 9018
Grand Forks, ND 58202-9018

2000-EERC-06-03 June 2000

DOE DISCLAIMER

ACKNOWLEDGMENT

This report was prepared with the support of the U.S. Department of Energy (DOE) National Energy Technology Laboratory Cooperative Agreement No. DE-FC26-98FT40320. However, any opinions, findings, conclusions, or recommendations expressed herein are those of the authors(s) and do not necessarily reflect the views of DOE.

EERC DISCLAIMER

TABLE OF CONTENTS

LIST OF FIGURES

LIST OF TABLES

SUBTASK 6.5 – SiAlON COATINGS OF SILICON NITRIDE AND SILICON CARBIDE

1.0 INTRODUCTION

The need for new engineering materials in aerospace applications and in stationary power turbine blades for high-efficiency energy-generating equipment has led to a rapid development of ceramic coatings. They can be tailored to have superior physical (high specific strength and stiffness, enhanced high-temperature performance) and chemical (high-temperature corrosion resistance in more aggressive fuel environments) properties than those of monolithic ceramic materials. Among the major chemical properties of SiAlON–Y ceramics are their good corrosion resistance against aggressive media combined with good thermal shock behavior.[1] The good corrosion resistance results from the yttria–alumina–garnet (YAG), $Al_5Y_3O_{12}$, formed during the corrosion process of SiAlON–Y ceramics in combustion gases at 1300°C. The interfacial chemical precipitation of the YAG phase is beneficial. This phase may crystallize in cubic and/or tetragonal modifications and if formed in SiAlON–Y ceramic may simultaneously generate residual stress. Also, this phase can contain a large number of point defects, which is a consequence of the large unit cell and complexity of the YAG structure because it has no close-packed oxygen planes. Therefore, the need exists to elucidate the corrosion mechanism of a multilayered barrier with respect to using SiAlON–YAG as a corrosion-protective coating.

Stress corrosion cracking in the grain boundary of a silicon nitride (Si_3N_4) ceramic enriched in a glassy phase such as SiAlON can significantly affect its mechanical properties. It has been suggested that the increased resistance of the oxynitride glass to stress corrosion is related to the increased surface potential of the fracture surface created in the more durable and highly cross-linked oxynitride glass network structure.[2] We expect that either increased or decreased surface potential of the intergranular glassy phase is brought about by changes in the residual stress of the SiAlON–Y ceramic and/or creation of a space-charge region at the SiAlON–YAG interface. Both features originate from a secondary phase of YAG formed during the SiAlON–Y glass corrosion process.

Conventional oxidation-protection coatings for metallic materials in high-temperature corrosive environments are typically formed by applying a slurry mixture to the surface followed by a high-temperature furnace cure. During the cure, the coating reacts with the alloy to form a layer typically 25 to 50 μm[3] thick. Generally, coating thickness is one critical microstructural parameter that influences its performance; therefore, its optimization is an important aspect of coating technology. The aim of the present research program is 1) to produce a thin SiAlON–YAG ceramic coating with a high quality of interface, 2) to understand the major experimental characteristics for creating a good bonding between a substrate and a thin coating, and 3) to explain why the $Al_5Y_3O_{12}$ phase increases SiAlON–Y ceramic alkali corrosion resistance.

To produce the SiAlON–Y coating on silicon nitride ceramic with a YAG layer, a slurry mixture of SiAlON–Y components was designed. The research program was extended to Y_2SiO_5 coating to get preliminary information on the Si_3N_4–Y_2SiO_5 interface microstructure. It was

expected that this phase would have a very low porosity. Generally, coatings that contain ductile phases such as Y_2SiO_5 can produce low-porosity coatings.

2.0 PHYSICOCHEMICAL PROPERTIES OF YAG

In the Y_2O_3–Al_2O_3 system, three compounds are found: $Al_5Y_3O_{12}$ with a garnet structure, $YAlO_3$ with a perovskite structure, and $Y_4Al_2O_9$ with a monoclinic structure. The $Y_4Al_2O_9$ phase appears to be unstable and decomposes into $Al_5Y_3O_{12}$ and Y_2O_3 phases.[4] The most thermodynamically stable phase is $Al_5Y_3O_{12}$ with cubic modification. Cubic YAG, $Al_5Y_3O_{12}$, has refractory and thermal properties similar to those of β–Al_2O_3.[5] When doped with rare-earth and/or transition metal ions, it has produced some of the most successful lasers.[6] A distinctive feature of YAG crystal is a high level of nonstoichiometry typically attributed to doubly ionized oxygen vacancies, $V^{\cdot\cdot}_O$, and usually formed by the removal of oxygen from the crystal into the gas phase:

$$O_O \Leftrightarrow V^{\cdot\cdot}_O + 2e + \tfrac{1}{2}O_2 \qquad \text{[Equation 1]}$$

where O_O and $V^{\cdot\cdot}_O$ represent oxygen ions on their normal sites and a double positively ionized oxygen vacancy, respectively, and e is an associated electron. The small excess of either Y_2O_3 or Al_2O_3 may increase the oxygen vacancy concentration.[7] There is no doubt that the concentration of oxygen vacancies and their mobilities will affect the ionic diffusion of all components. In general, vacancies have higher mobility than the associated solutes and defect complexes.[8, 9] The study of transport properties as a function of temperature and oxygen partial pressure confirms a mixed ionic–electronic conductivity with a strong p-type (positive) component at high temperatures. It was found that the addition of calcium dopant creates negatively charged acceptors that with positively charged oxygen vacancies form low-mobility complexes.

3.0 EXPERIMENTAL PROCEDURE

3.1 Sintering Procedure for YAG and SiAlON–Y Coating on Silicon Nitride Substrate and Thermal Expansion Coefficient Tests

3.1.1 Sintering of $Al_5Y_3O_{12}$ Phase and Thermal Expansion Coefficient Tests

Pressureless sintering of the $Al_5Y_3O_{12}$ phase was accomplished using 0.63- and 0.37-mole fractions of Al_2O_3 and Y_2O_3, respectively, at 1600°C for 15 hr. After sintering, the sample was cooled as the furnace cooled to room temperature. Prior to sintering, powders of alumina and yttria were stirred in water-free propanol using a blender for 1 hour and dried at 150°C. X-ray diffraction (XRD) tests of the $Al_5Y_3O_{12}$ specimen showed the existence of both cubic and tetragonal phases. There has been no information in the available literature on coefficients of thermal expansion (CTEs) for the tetragonal phase of the $Al_5Y_3O_{12}$. Thus, the CTEs for both tetragonal and cubic forms of $Al_5Y_3O_{12}$ phase were measured from room temperature up to

1400°C using XRD and applied in estimating the residual stresses generated at the SiAlON–$Al_5Y_3O_{12}$ interface.

The CTE for $Al_5Y_3O_{12}$ was measured using a high- temperature Philips X'Pert MPD x-ray diffractometer equipped with Cu Kα radiation in the temperature range of 20° to 1400°C. Data were collected at 0.01° step scanning mode in a 10°–70° 2θ range, counting 3s/step. The powdered $Al_5Y_3O_{12}$ sample was mounted on the Pt–Rh heating strip, and the sample temperature was measured using a Type S thermocouple spot- welded to the bottom of the heater strip. All experiments were run in air.

3.1.2 Formation of SiAlON–Y Coatings on Silicon Nitride Substrate

The SiAlON–Y coatings on silicon nitride substrates were produced using a powder sintering method. Two different procedures for the powder preparation were pursued. The relative molar fraction of all components in the coating was designed to be the same in both procedures.

3.1.2.1 Method I

Si_3N_4 bars were covered by a powder mixture of silicon nitride, aluminum oxide, aluminum nitride, and yttrium chloride hexahydrate in the following mole fractions: Si_3N_4 = 0.273, Al_2O_3 = 0.273, AlN = 0.273, $YCl_3 \cdot 6H_2O$ = 0.179 and sintered at 1600°C for 5 hr in a nitrogen atmosphere with 1 vol% hydrogen. The addition of 0.179 mole fraction of $YCl_3 \cdot 6H_2O$ yielded 0.089 mole fraction of Y_2O_3 after its decomposition and oxidation and 0.306 mole fraction of the remaining components. The mixture was then vacuum-dried at 150°C before sintering. It was assumed that at this temperature the $YCl_3 \cdot 6H_2O$ phase melts (T_m = 100°C) and uniformly distributes over the remaining ceramic components. Prior to sintering, the mixture was first annealed in air at 400°C for 60 min to decompose and oxidize the $YCl_3 \cdot 6H_2O$ to Y_2O_3. It was assumed that this procedure may improve the final microstructure of the SiAlON ceramic coating. Considerable attention has been given 1) to oxidation behavior of AIN during $YCl_3 \cdot 6H_2O$ decomposition in air and 2) chemical reactivity of volatile chlorine components with AIN and formation of volatile aluminum chloride components.

To date, several studies have been performed on the effects of oxygen and moisture on the stability of AlN powder.[10–13] These indicate that the oxidation of AlN was usually initiated at about 600°C. Similar evidence on AlN powder oxidation was recorded in our test (see Appendix A). Therefore, it was assumed that the stoichiometry of the AlN phase would be preserved during a short time of $YCl_3 \cdot 6H_2O$ decomposition and oxidation to Y_2O_3 at 400°C in an air atmosphere.

The chemical stability of AlN in the presence of chlorine components was verified both experimentally and using chemical thermodynamic calculations. It was found that at a low decomposition temperature such as 400°C and oxidation of $YCl_3 \cdot 6H_2O$ to Y^2O^3 cause the formation of volatile aluminum chlorides with a sublimation temperature of about 180°C.

3.1.2.2 Method II

Si_3N_4 bars were covered by a powder mixture of silicon nitride, aluminum oxide, aluminum nitride, and yttrium oxide in the following mole fractions: Si_3N_4 = 0.306, Al_2O_3 = 0.306, AlN = 0.306, Y_2O_3 = 0.08 and sintered at 1600°C for 5 hr in a nitrogen atmosphere with 1 vol% of hydrogen. After sintering, samples were cooled as the furnace cooled to room temperature. The equimolar amounts of Si_3N_4, Al_2O_3, and AlN prepared prior to high-temperature sintering should stabilize the important single-phase β-SiAlON, and a small addition of yttria should have a positive effect on both sintering of β-SiAlON and its fracture toughness.[14] The starting powders were carefully weighed and stirred in water-free propanol using a blender for 3 hr. The mixture was then vacuum-dried at 150°C before sintering.

3.1.3 Formation of Y_2SiO_5 Coating on Silicon Nitride Substrate

A coating of Y_2SiO_5 on a Si_3N_4 bar was cured at 1600°C for 5 hr in a nitrogen atmosphere. Prior to the sintering test, powders of 0.5 mole of alumina and 0.5 mole of yttria, both with a particle size of 0.05 mμ, were synthesized at 1500°C for 15 hr, and the produced yttrium silicate was ground to a particle size below 38 μm. Again, the starting powders were carefully weighed and stirred in water-free propanol using a blender for 5 hr. The mixture was then vacuum-dried at 150°C before sintering. This new component for the formation of a protective coating on Si_3N_4 ceramic was designed to replace the aluminum-modified polycarbosilane method described elsewhere.[15] Our preliminary synthesis test using the aluminum-modified polycarbosilane method showed the formation of large pores, easy observed under an optical microscope at low magnification, that were difficult to remove from the coating under sintering conditions. Recent results indicate that this new oxide coating could be successfully used as an oxidation protection coating for SiC structural ceramic.[16]

3.2 Surface Preparation of Si_3N_4 Substrate

Surface preparation of the substrate is one of the important steps prior to the coating formation. It may also determine coating adhesion independently of the coating components' distribution. Accordingly, Si_3N_4 bars were polished and cleaned with ethanol.

3.3 Coating Characterization

The morphology of the substrate–coating interface was examined on polished cross-sectioned samples using scanning electron microscopy (SEM), and point count chemical analysis was performed by energy-dispersive x-ray analysis coupled with SEM to evaluate yttrium and aluminum distribution in the coating.

4.0 RESULTS AND DISCUSSION

4.1 Thermal Expansion Coefficients of YAG and SiAlON–YAG Stress Development

In our previous report, it was found that the outward diffusion of yttrium atoms into the surface of SiAlON ceramic could give rise to the precipitation of yttrium-rich oxide barriers to corrosion-active components at 1300°C. This layer was most likely formed by 1) a dissolution of intergranular yttrium-rich phases into the silicate melt, 2) the diffusion of solute into the melt surface, 3) its chemical reaction with oxygen, and 4) reprecipitation at the surface of β-SiAlON–Y ceramics as aluminum yttrium garnet and yttrium silicate.

Crystallization of a thin boundary layer of both $Al_5Y_3O_{12}$ and $Y_{4.67}(SiO_4)_3O$ phases near the surface of the SiAlON ceramic may produce strain mismatches from resulting volume changes, thermal expansion anisotropy of noncubic phases, and thermal expansion mismatch that can constrain the motion of sodium ions in SiAlON–Y ceramics. Thus, it was important to determine the volume changes in unit cell and thermal expansion properties of aluminum yttrium oxide and introduce them into the discussion of both stresses generated at the $Al_5Y_3O_{12}$–SiAlON interface and their effect on the corrosion of β-SiAlON–Y ceramics.

XRD patterns show the existence of two high-temperature $Al_5Y_3O_{12}$ forms crystallized in both cubic and tetragonal systems. The results of high-temperature x-ray tests are listed in Tables 1 and 2. The CTE for the cubic form of $Al_5Y_3O_{12}$ is

$$\alpha = 8.40 \times 10^{-6}\ \text{deg}^{-1}\ (\pm 0.29 \times 10^{-6}\ \text{deg}^{-1}),$$

and for the tetragonal form is

$$\alpha(a) = 4.4 \times 10^{-6}\ \text{deg}^{-1}\ (\pm\ 0.5 \times 10^{-6}\ \text{deg}^{-1})\ \text{and}\ \alpha(c) = 11.3 \times 10^{-6}\ \text{deg}^{1}\ (\pm 1.5 \times 10^{-6}\ \text{deg}^{-1}).$$

The α coefficients for the powdered tetragonal $Al_5Y_3O_{12}$ form can be directionally averaged over the range 20° to 1400°C, $\alpha_{avg} = (2\alpha_a + \alpha_c)/3$, giving a CTE of $\alpha = 6.8 \times 10^{-6}\ \text{deg}^{-1}$. The CTE for the cubic form of $Al_5Y_3O_{12}$ has been determined by Gupta and Valentich[17] using a dilatometric technique. For a polycrystalline sample with 5% porosity, the coefficient was $8.9 \times 10^{-6}\ \text{deg}^{-1}$, and for single crystallite, it was $8.0 \times 10^{-6}\ \text{deg}^{-1}$.

The differences in values for thermophysical and mechanical properties in the substrate and coating can lead to internal stresses. The total stress of a coating, σ_T, comprises several different contributions:

TABLE 1

Interplanar Spacings (d-values) for $Al_5Y_3O_{12}$ Cubic Form at Different Temperatures

Temp., °C	d ( )				Cell Parameter ( )	Unit Cell Volume ( )^3
	(420)	(422)	(431)	(521)		
20	2.6805	2.4485	2.3512	2.1901	11.992 ± 0.004	1724.546
200	2.6845	2.4505	2.3565	2.1922	12.008 ± 0.008	1731.458
300	2.6875	2.4521	2.3571	2.1939	12.016 ± 0.003	1734.921
400	2.6892	2.4559	2.3598	2.1958	12.029 ± 0.004	1740.558
500	2.6935	2.4588	2.3613	2.1971	12.042 ± 0.006	1746.208
600	2.6968	2.4615	2.3628	2.1997	12.054 ± 0.006	1751.433
800	2.6998	2.4652	2.3668	2.2050	12.074 ± 0.006	1760.166
900	2.7015	2.4672	2.3688	2.2060	12.083 ± 0.004	1764.105
1000	2.7035	2.4698	2.3705	2.2086	12.093 ± 0.005	1768.488
1100	2.7058	2.4703	2.3728	2.2091	12.101 ± 0.002	1772.000
1200	2.7094	2.4721	2.3753	2.2108	12.112 ± 0.005	1776.837
1300	2.7100	2.4734	2.3760	2.2111	12.116 ± 0.005	1778.598
1400	2.7115	2.4746	2.3773	2.2128	12.123 ± 0.003	1781.683

TABLE 2

Interplanar Spacings (d-values) for $Al_5Y_3O_{12}$ Tetragonal Form at Different Temperatures

Temp., °C	d ( )						"a" ( )	"c" ( )	Unit Cell Volume ( )^3
	(220)	(211)	(300)	(301)	(002)	(102)			
20	2.6514	2.6223	2.4925	2.1490	2.1130	2.0403	7.488	4.226	236.952
200	2.6538	2.6283	2.4943	2.1512	2.1137	2.0431	7.494	4.235	237.838
300	2.6540	2.6299	2.4972	2.1533	2.1145	2.0450	7.500	4.239	238.444
400	2.6539	2.6304	2.4980	2.1544	2.1151	2.0479	7.500	4.242	238.613
500	2.6545	2.6311	2.4987	2.1550	2.1189	2.0495	7.502	4.246	238.965
600	2.6556	2.6315	2.4996	2.1579	2.1232	2.0519	7.504	4.248	239.205
800	2.6598	2.6416	2.5029	2.1608	2.1280	2.0566	7.515	4.268	241.036
900	2.6601	2.6448	2.5042	2.1628	2.1304	2.0575	7.519	4.275	241.689
1000	2.6629	2.6467	2.5065	2.1640	2.1321	2.0613	7.525	4.278	242.244
1100	2.6631	2.6475	2.5071	2.1646	2.1368	2.0619	7.527	4.284	242.713
1200	2.6637	2.6481	2.5085	2.1665	2.1375	2.0644	7.529	4.285	242.899
1300	2.6637	2.6455	2.5091	2.1666	2.1388	2.0667	7.531	4.286	243.085
1400	2.6640	2.6527	2.5110	2.1669	2.1410	2.0673	7.533	4.294	243.668

$$\sigma_T = \sigma_{IS} + \sigma_E \qquad \text{[Equation 2]}$$

where σ_{IS} is an internal stress and σ_E is a stress due to external forces.

Crystallization of a thin boundary layer of $Al_5Y_3O_{12}$ phase near the surface of SiAlON–Y ceramics introduces a residual stress field, resulting from the misfit strain caused by 1) the thermal

expansion mismatch and 2) elastic moduli between the precipitates and the matrix at the corrosion temperature. The CTE of SiAlON–Y glasses containing 6 at% of nitrogen is around $4 \times 10^{-6}/°C$, and this coefficient increases with decreasing nitrogen content so that a pure oxide glass corresponds to $7.5 \times 10^{-6}/°C$.[18] Because the CTE of the $Al_5Y_3O_{12}$ phase is higher than that of the SiAlON matrix, $\Delta\alpha = \alpha(Al_5Y_3O_{12}) - \alpha(SiAlON–Y)$ has a positive value, and this suggests that the $Al_5Y_3O_{12}$ precipitates are under an axial tensile stress, while above the interface the axial stresses become compressive.[19–22] In the classical models, it is generally agreed that tensile stresses normal to the $Al_5Y_3O_{12}$–SiAlON interface occur within a small region, while compressive stress persists to distances below and above the $Al_5Y_3O_{12}$ layer. Both the tensile stress in the thin boundary layer of $Al_5Y_3O_{12}$ and compressive stresses above and beneath this layer increase with the increase of precipitate thickness.[23]

Generally, the SiAlON–YAG interface may exhibit a singular behavior toward sodium mass transport and affect its diffusion 1) through created tensile and compressive stresses, and 2) through the propagated space-charge region in the $Al_5Y_3O_{12}$ layer and sodium surface segregation.

4.2 The Effect of Stress Generated in YAG Precipitates on the Corrosion Reduction of SiAlON–Y Ceramics

Generation of compressive residual stress at the SiAlON–YAG interface may have a beneficial effect on its alkali corrosion resistance. The average flux of sodium ions from the gas–solid contact areas to the $Al_5Y_3O_{12}$ precipitates can be briefly described as follows:

$$J \quad - D\sigma(\delta N_{Na}/\delta z) \qquad \text{[Equation 3]}$$

where D is the diffusion coefficient under the unstressed condition, σ is a stress parameter, and $\delta N_{Na}/\delta z$ is the axial gradient of the sodium ions.[24] According to Equation 3, the sodium ion flux is accelerated by the tensile internal stress (positive sign) and is suppressed by the compressive internal stress (negative sign). The thermodynamic factor in the mass transport in solids is coupled with chemical potential gradients, mostly related to the gradient in concentration of solute. More complicated situations arise if the diffusion of solute is affected by external thermodynamic activity such as stress. A typical example would be the diffusion of sodium ions under the compressive internal stress generated at the SiAlON–$Al_5Y_3O_{12}$ precipitate interface. If the generated compressive stress is lower than a critical value, the reduction of sodium diffusion into the bulk of SiAlON ceramics at 1300°C may not be distinguished.

SiAlON ceramic at above 1300°C is considered to be a viscoelastic material exhibiting structural relaxation.[25] The amorphous part of SiAlON formed above and beneath the $Al_5Y_3O_{12}$ precipitates should enable relaxation of the internal tensile and compressive stresses. It is questioned whether the elastic compressive stress generated at the $Al_5Y_3O_{12}$–SiAlON interface should be partially preserved and whether this is essentially a function of aluminum yttrium garnet film thickness. It is possible that the resulting internal compressive stress cannot significantly build

up a thermodynamic barrier for sodium ion diffusion into SiAlON–Y ceramics if the composition of the silicate phase reaches a local dynamic equilibrium.

4.3 The Effects of Positively Ionized Oxygen Vacancies in YAG Precipitates on the Corrosion Reduction of SiAlON–Y Ceramics

As mentioned in Section 2.0, double positively ionized oxygen vacancies, $V^{\cdot\cdot}_O$, and associated electrons are the major defects in the $Al_5Y_3O_{12}$ phase. The occurrence of tensile stresses in the $Al_5Y_3O_{12}$ grain-boundary region may additionally increase oxygen vacancy concentration and particularly elastic energy. The elastic energy may extend up to several lattice constants from the grain boundary, and its magnitude is related to the size misfit, $\Delta\alpha$.[23] Usually, the vacancy concentration in the grain boundaries is higher than that in the bulk of grains, and this creates the space-charge region.[26] In the bulk, the vacancy concentration only depends on the entropy and condition of charge neutrality, while in the surface, it also depends on the elastic energy and kinetic processes related to interfacial reactions. The space-charge region is overwhelmingly positive and is a function of the distribution of vacancies. Generally, material transport is required to redistribute the charge species. Spatial distribution of positively ionized oxygen vacancies in the $Al_5Y_3O_{12}$ precipitates can create a potential barrier for sodium ion diffusion in grain boundaries. This can give rise to the corrosion reduction of SiAlON–Y ceramics above 1300°C. Finally, the increase in space-charge region with YAG thickness increases the potential barrier for sodium ion diffusion with corrosion time, and this suggests that sodium ions may migrate in opposite directions against their coupled chemical potential gradients.

To help explain the diffusion of sodium ion reduction at 1300°C, thermodynamic calculations using the FACT code[27] were performed to show that the partial pressure of sodium components such as NaOH, Na, and Na_2SO_4 over liquid $Na_2O \cdot 2SiO_2$ phase can increase if vaporization temperature is raised up from 1200° to 1300°C. In these calculations, $Na_2O \cdot 2SiO_2$ was applied rather than SiAlON–Y and $Al_5Y_3O_{12}$ phases because of lack of thermodynamic data on these phases. Also, oxygen vacancy content in the $Al_5Y_3O_{12}$ phase increases with temperature, which may also increase the space-charge region.

4.4 SiAlON–Y and Y_2SiO_5 Coatings on Si_3N_4 Ceramic

Figure 1 illustrates the cross-sectional microstructure of SiAlON–YAG coating on Si_3N_4 ceramic produced during the sintering of a powder mixture of silicon nitride, aluminum oxide, aluminum nitride, and yttrium chloride hexahydrate at 1600°C. The thickness of the coating is about 10 mμ. Of particular interest is the coating–ceramic interface. First, substrate and coating are continuous in at least one dimension, suggesting a good adhesion at the interface. Unfortunately, the coating contains pores, likely formed during the low-temperature yttrium chloride decomposition in an air atmosphere and the formation of volatile aluminum chlorides. The size of the pores was not reduced enough during the sintering process because of 1) the high viscosity of SiAlON–Y melt and 2) the low thickness of the coating. In some coatings such as ZrO_2/Y_2O_3, the presence of fine pores could increase its thermal shock resistance as a result of expansion tolerance of the coating.[28,29] Also, their Young module could decrease with the

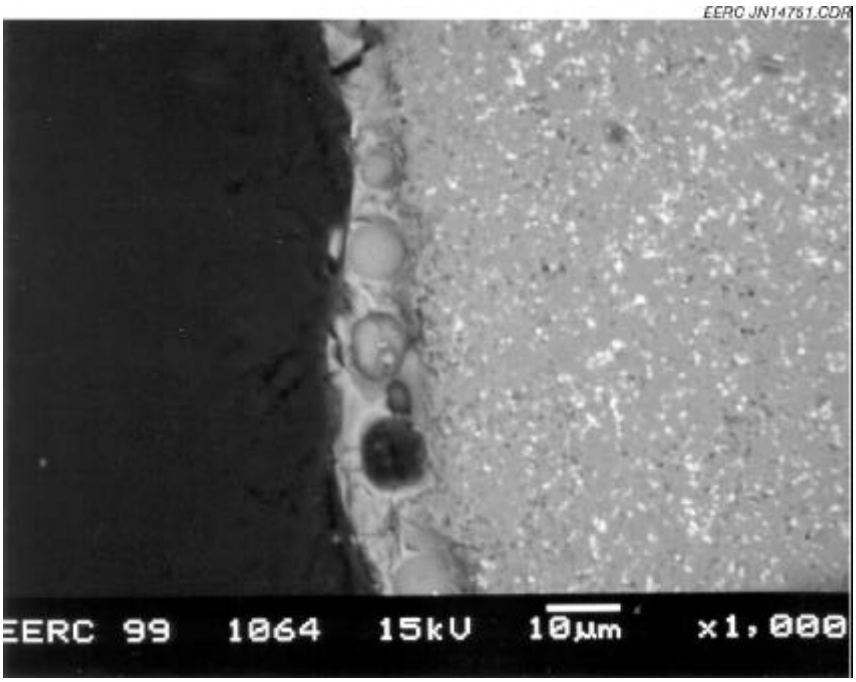

Figure 1. Cross-sectional view of the SiAlON–YAG coating on Si_3N_4 ceramic.

increase in porosity. The surface morphology of the SiAlON–YAG coating also shows a large precipitation of YAG phase (Figure 2). The point count chemical analysis made across the coating shows a large yttrium and aluminum oxide content near the coating surface (Figure 3). There are no microcracks at the Si_3N_4 ceramic coating and SiAlON–YAG interfaces, and this results from a low residual stress factor. The applied stress resulting from the difference in CTEs between substrate and coating below the temperature of glass transformation is very small. Thus, the ceramic coating during its cooling down to the temperature of glass transformation behaves as a viscoplastic material that involves a diffusion of matter from the interface under relative compression to the areas under extension.

A great reduction of pore size in SiAlON–Y coating is observed when $YCl_3 \cdot 6H_2O$ is replaced by Y_2O_3 prior to sintering at 1600°C (Figure 4). Essentially, the micropores are observed only in the silicon nitride bar. From the above results, we may conclude that the presence of any chloride-derived components in SiAlON–Y ceramic may increase their porosity and reduce aluminum content in SiAlON ceramics from that applied for sintering.

A distinctive feature of an ideal coating microstructure is evident in Y_2SiO_5 coating on silicon nitride substrate (Figure 5). Conventional coatings consist of multilayers of different materials designed to seal cracks by forming glassy phases. The yttrium silicate coating possesses the characteristics of an ideal glassy coating. This coating was successfully applied as an oxidation protection coating for C/SiC ceramic. The factor that currently precludes the use of carbon fiber-reinforced carbide (C/SiC) in high-temperature structural applications such as gas turbine engines is the oxidation of carbon fibers at temperatures greater than 400°C.[16]

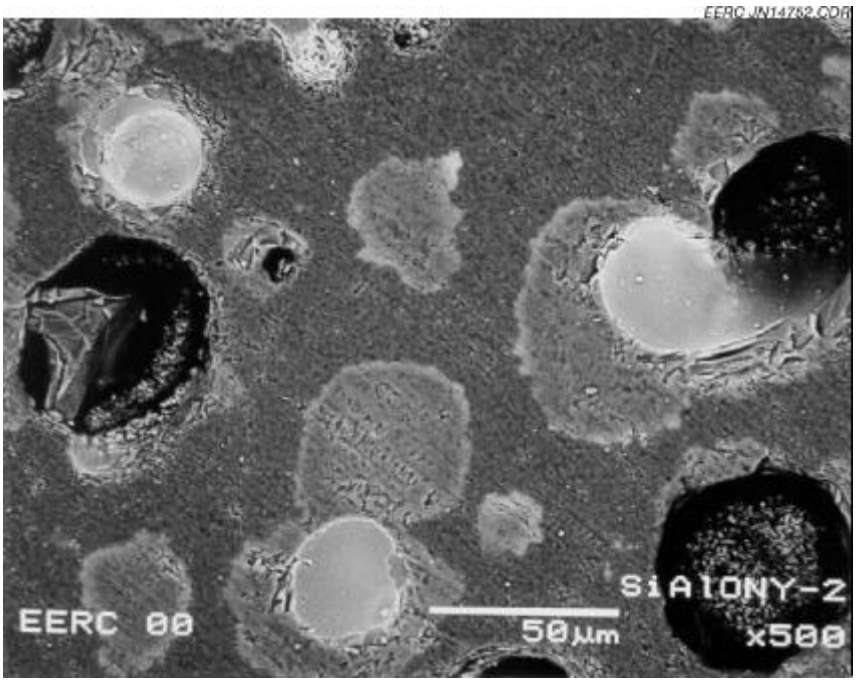

Figure 2. Surface morphology of SiAlON–YAG coating on Si_3N_4 ceramic.

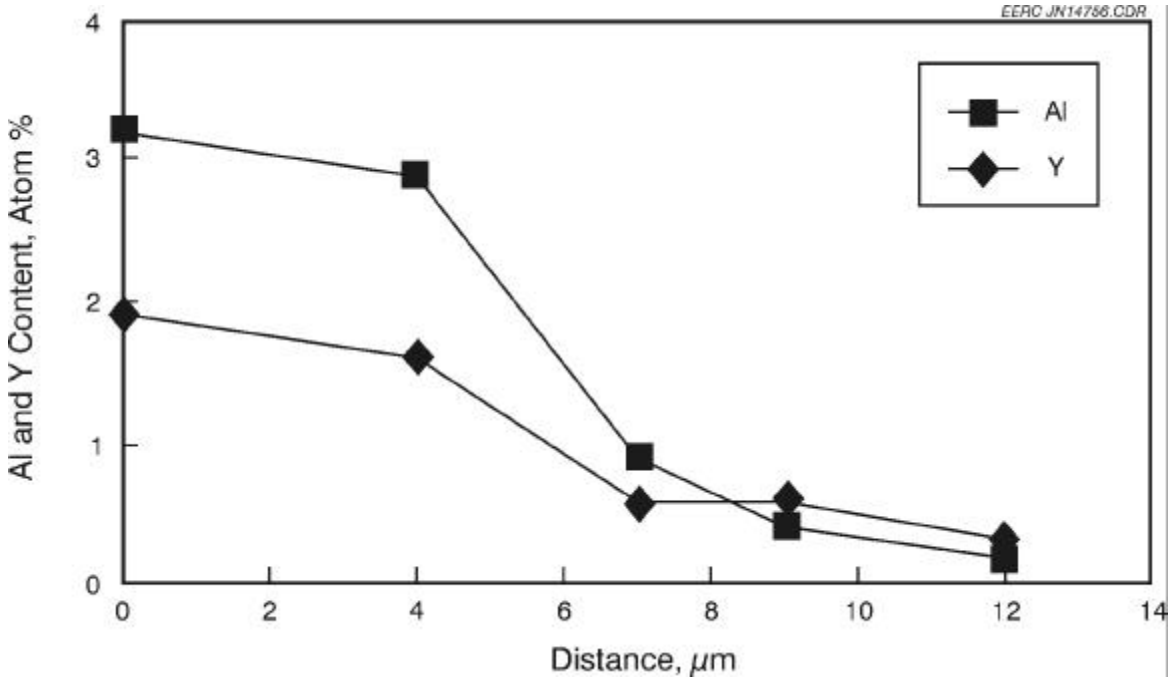

Figure 3. Cross-sectional Y and Al chemical distribution in SiAION-Y coating on Si_3N_4 ceramic.

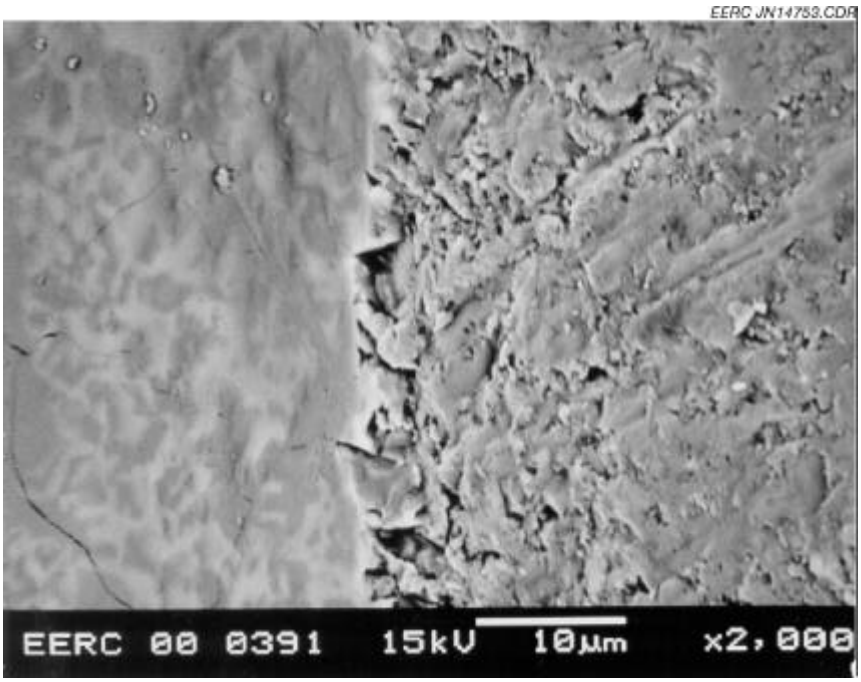

Figure 4. Surface morphology of SiAlON–Y coating on Si_3N_4 ceramic after changes in coating technology.

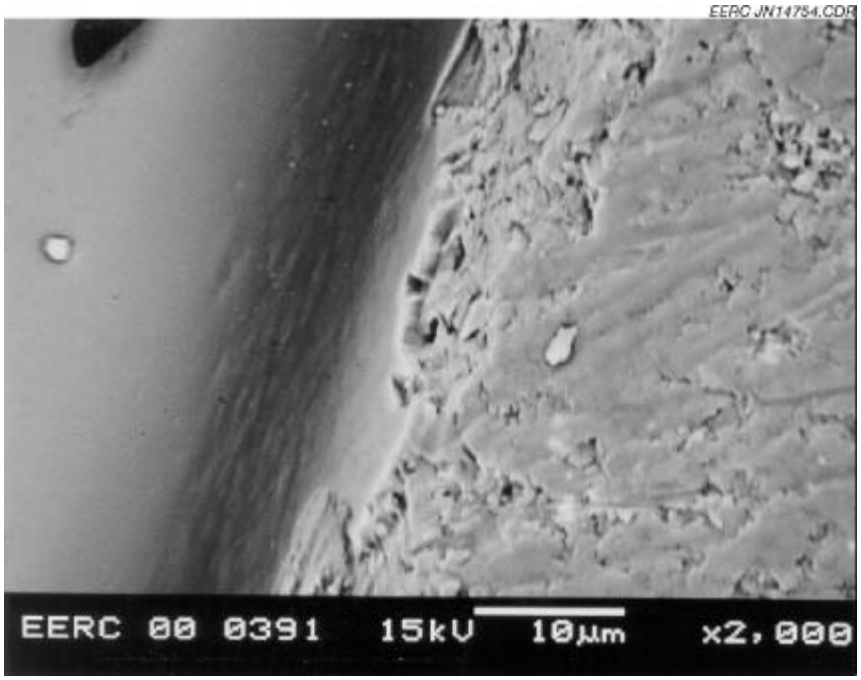

Figure 5. Cross-sectional view of the Si_3N_4–Y_2SiO_5 coating.

CONCLUSIONS

It is demonstrated that β-SiAlON–Y and Y_2SiO_5 coatings on silicon nitride ceramics form well-adhered layers. Conventional coatings consist of multilayers of different materials to create protective properties for use in combustion environments. These coatings contain a layer of two phases and perform well.

SUGGESTIONS FOR FUTURE WORK

The formation of protective layers requires high temperature and a long experimental time. Industry is interested in a good-quality protective layer obtained in a short fabrication time. Plasma spray technology is considered a potential method of reducing technology time and is one of the most versatile methods of applying coatings. Understanding the link between processing parameters and final deposit properties is one of the keys to ensuring coating performance and process economy. Therefore, before applying SiAlON–Y and Y_2SiO_5 coatings as protective layers for selected structural ceramics and alloys such as aircraft alloy $TiAl_6V_4$ and nickel-based alloys for stationary turbine blades, we propose to use the plasma technique to define the technical conditions for the formation of those coatings on silicon nitride, silicon carbide, and selected metallic alloys. This suggestion is based on our discussion with Alupro Company from the Netherlands made last year and on a literature search.

REFERENCES

1. Nowok, J.W., SiAlON coatings for alkali-resistant silicon nitride, Cooperative Agreement No. DE-FC21-93MC30097, Jan 1997

2. Bhatnagar, A., Hoffman, M.J. and Dauskardt, R.H., Fracture and subcritical crack-growth of Y-Si-Al-O-N glasses and Si_3N_4 ceramics. J. Am. Ceram. Soc. **83** (2000) 585–96

3. Cunnington, G.R., Clark, R.K. and Robinson J.C., Thermal coatings for titanium–aluminum alloys, NASA Technical Memorandum 107760, April 1993

4. Yamane, H., Omori, M. Okubo, A. and Hirai, T., J. Am. Ceram. Soc. **76** (1993) 2382–2884

5. Bates, J.L. and Garnier, J.E., J. Am. Ceram. Soc. **64** (1981) C138–141

6. Rotman, S.R., Tuller, H.L. and Warde, C., A., J. Appl. Phys., **71** (1992) 1209–1214

7. Sakaguchi, I., Haneda, H., Tanaka, J. and Yanagitani, T., J. Am. Ceram. Soc., **79** (1996) 1627–32

8. Rotman, S.R., Tuller, H.L. and Warde, C., A., J. Appl. Phys., **57** (1985) 1951–1955

9. Yan, M.F., Cannon, R.M. and Bowen, H.K., J. Appl. Phys., **54** (1983) 764–778

10. Katnani, A.D. & Papathomas, K.I., J. Vac. Sci. Technol. **A5** (1987) 1335–1340

11. Suryanarayana, D., J. Am. Ceram. Soc. **73** (1990) 1108–10

12. Solmon, H., Robinson, D. and Dieckmann, R., J. Am. Ceram. Soc. **77** (1994) 2841–2848

13. Nocolaescu, I.V., Tardos, G. and Riman, R.E., J. Am. Ceram. Soc. **77** (1994) 2265–2272

14. Mieskowski, D.M. & Sanders, W.A., J. Am. Ceram. Soc. **68** (1985) C-160–163

15. Soraru, G.D., Ravagni, A. and Campostrini, R., J. Am. Ceram. Soc. **74** (1991) 220–223

16. Webster, J.D., Westwood, MR., Hayes, F.H., Day, R.J., Taylor, R., Duran, A., Aparicio, M., Rebstock, K. and Vogel, W.D., Key Engineering Materials, Proc 1997 Conf and Exhibition of the European Ceramic Society, 22–26 June 1997, v. 132–136, 1997, Versailles, Fr. Trans. Tech. Publ. Clasusthahl-Zellerfeld Germany, pp. 1641–1644

17. Gupta, T.K. and Valentich J., J. Am. Ceram. Soc. **54** (1971) 355–356

18. Ekström, T, Mat. Res. Soc. Symp. Proc., **287** (1993) 121–132

19. Rekhson, S.M., J. Am Ceram. Soc. **76** (1993) 1113–1123

20. Kessler, H. Kleebe, H.J., Cannon, R.W. and Pompe, W., Acta Metall. Mater. **40** (1992) 2233–2245

21. Cao, C.H., Thouless, M.D. and Evans, A.G., Acta Metall. **36** (1988) 2037–2046

22. Hampshire, S., Mat. Res. Soc. Symp. Proc. **287** (1993) 93–104

23. Person, J., Ekström, T., Per-Olov Kall and Nygren, M., J. Europ. Ceram. Soc. **11** (1993) 363–373

24. Patel, J.K. and Thomson, D.P., Brit. Ceram. Trans. J. **87** (1988) 70–78

25. Wang, J.N. and Shimamoto, T., Mater. Sci. Enging **A188** (1994) 175–184

26. Brown, K.R. and Bonnell, D.A., J. Am. Ceram. Soc., **82** (1999) 2423–2430, and 2431–2441

27. Bale, C.W., Pelton, A.D. and Thomson, W.T., Facility for the Analysis of Chemical Thermodynamics program (FACT), École Polytechnique de Montréal, 1999

28. Steffens, H.D., Babiak, Z. and Brandl, W., Proc. Fourth Natl. Thermal Spray Conf., Pittsburgh, PA, USA, 4–10 May 1991, Thermal Spray Coatings, ASM Intl., Materials Park, 1992, pp. 289–294

29. Knotek, O., Loffler, F. and Beele, W., Mat. Res. Symp. Proc., **287** (1993) 539–545

APPENDIX A

THERMOGRAVIMETRIC ANALYSIS OF ALUMINUM NITRIDE OXIDATION

Thermogravimetric Analysis of Aluminum Nitride Oxidation

The sample used for thermogravimetric analysis (TGA) was a powder with an average particle size of 6µ manufactured by the Aldrich Chemical Company, Inc. TGA oxidation was monitored using a Dupont 951 TGA with a 9900 thermal analyzer as changes in a sample weight with temperature at constant heating rate of 3deg/min. The sample size was kept constant at approximately 40 mg. The TGA microbalance is sensitive within ±0.01 mg. Figure A-1 illustrates the weight change as a function of temperature. Notice that for temperatures below 700°C, no weight change is observed. For temperatures between 750° and 900°C, the oxidation involves the formation of oxynitrides.

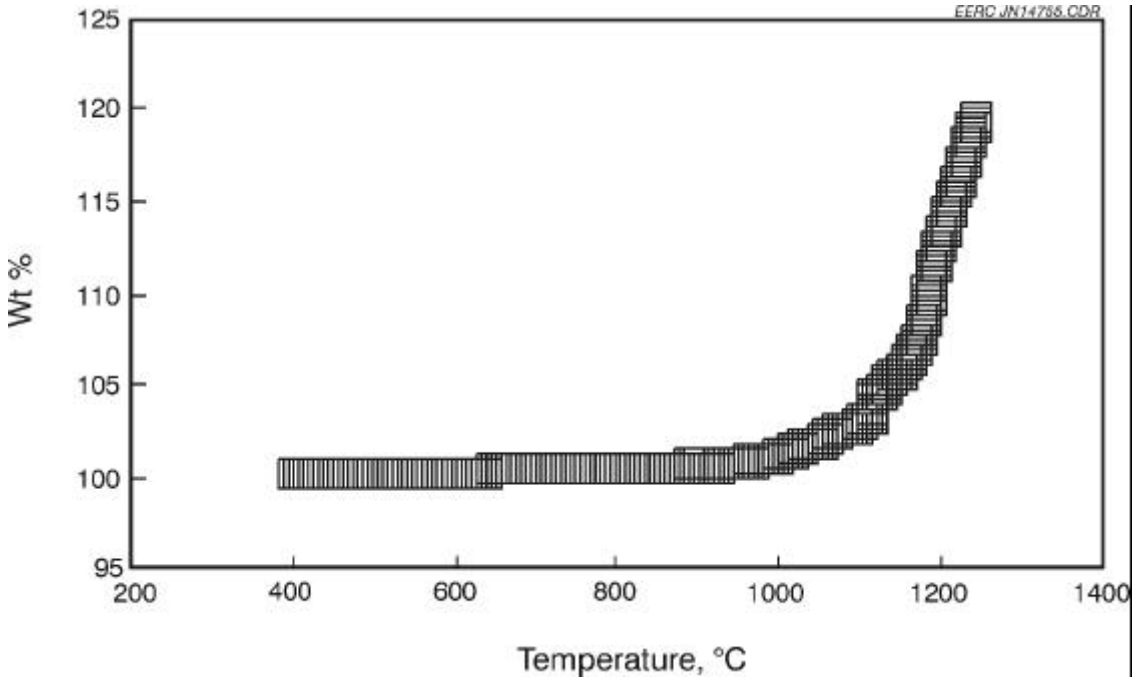

Figure A-1. TGA curve for AlN powder oxidized in air.